THE JOURNAL OF PHYSICAL CHEMISTRY B

ARTICLE

pubs.acs.org/JPCB

DFT Energy Optimization of a Large Carbohydrate: Cyclomaltohexaicosaose (CA-26)

Udo Schnupf[†] and Frank A. Momany*[,‡]

[†]Department of Food Sciences, Cornell University, Ithaca, New York 14853, United States

[‡]Plant Polymer Research, USDA, ARS, National Center for Agricultural Utilization Research, 1815 North University Street, Peoria, IL 61604, United States

ABSTRACT: CA-26 is the largest cyclodextrin (546 atoms) for which refined X-ray structural data is available. Because of its size, 26 D-glucose residues, it is beyond the scope of study of most ab initio or density functional methods and to date has only been computationally examined using empirical force fields. The crystal structure of CA-26 is folded like a figure "8" into two 10 D-glucoses long antiparallel left-handed V (Verkleisterung)-type helices with a "band-flip" and "kink" at the top and bottom of the helices. DFTr methods were applied to CA-26 to determine if a carbohydrate molecule of this size could be geometry optimized and if it would show structural variances from application of dispersion and/or solvation. The DFTr reduced basis set method developed by the authors uses 4-31G on the carbon atoms of the glucose rings and 6-31+G* on all other atoms. B3LYP is the density functional used to successfully optimize CA-26, and other density functionals were then applied, including a self-consistent charge density functional tight binding (SCC-DFTB) method and the B97D (dispersion-corrected) and B97D-PCM (dispersion + implicit solvent) methods. Heavy atom coordinates were taken from one X-ray structure, fitted with hydrogen atoms, and geometry optimized using PM3 followed by B3LYP/6-31+G*/4-31G optimization. After optimization, the heavy atom rms deviation of the optimized DFTr (B3LYP) structure to the crystal structure was 0.89 Å, the rmsd of the B97D optimization was 1.38 Å, that for B97D-PCM was 0.95 Å, and that for SCC-DFTB was 0.94 Å. These results are very good considering that no explicit water molecules were included in the computational analysis and there were ~32−38 water molecules around each CA-26 molecule in the crystal structure. Tables of internal coordinates and puckering parameters were compared to the X-ray structures, and close correspondence was found.

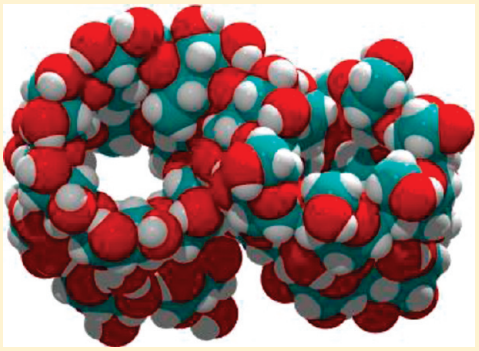

INTRODUCTION

The structure of CA-26[1−5] has sparked an interest in crystal structure versus solution conformation because it was shown[6] that the solution conformation of CA-26 could not be simulated by its X-ray crystal structure. Further, because of its band-flip, kink, and V-helix secondary structures, as well as its hydrogen bonding patterns, (see Figure 1) it tests the ability of computational chemistry to define the forces that are at work to stabilize this conformation in the solid state. In a previous publication,[7] band-flip and kink conformations in maltotetraose were examined by density functional (DFT) methods, and the relative energy of this unusual "flipped" conformation was obtained. However, in order to examine a structure of the CA-26 size using DFT methods, it was necessary to create and test computational procedures that would allow such calculations in a reasonable amount of computer resources, that is, memory space and time, and yet retain the reduced but significant accuracy found using larger basis sets. This was accomplished for the DFTr method[8] in several ways by noting that the carbon atoms in the sugar rings were adequately accounted for by a smaller basis set, that is, 4-31G, than had been previously used, that is, 6-31+G*. The ~3-fold reduction in computing time and significant reduction in memory requirements found from this change made it possible to consider that a molecule of the CA-26 size could be studied by these electronic methods. Once a DFTr optimization was carried out on CA-26, other DFTr methods were applied to the optimized structure, including dispersion-corrected and implicit solvation methods. Optimization of CA-26 was previously carried out in this laboratory using empirical AMB06C potentials.[9]

The size of the CA-26 molecule makes it an excellent test case for the application of the DFTr methods (see Table 1). For example, B97D is an effective scheme for describing dispersion interactions, without losing the efficiency of the DFTr methodology by the addition of semiempirical dispersion terms, that is, by addition of long-range attractive pair potentials and a short-range cutoff.[10] Although the conformation of this molecule is defined by covalent and hydrogen bonding, the effect of dispersion on, for example, the compression of the helices may be important; thus, we examine results from the dispersion-corrected method. Another addition to the DFTr method is the D-PCM, or

Special Issue: Harold A. Scheraga Festschrift

Received: September 15, 2011
Revised: November 29, 2011
Published: December 08, 2011

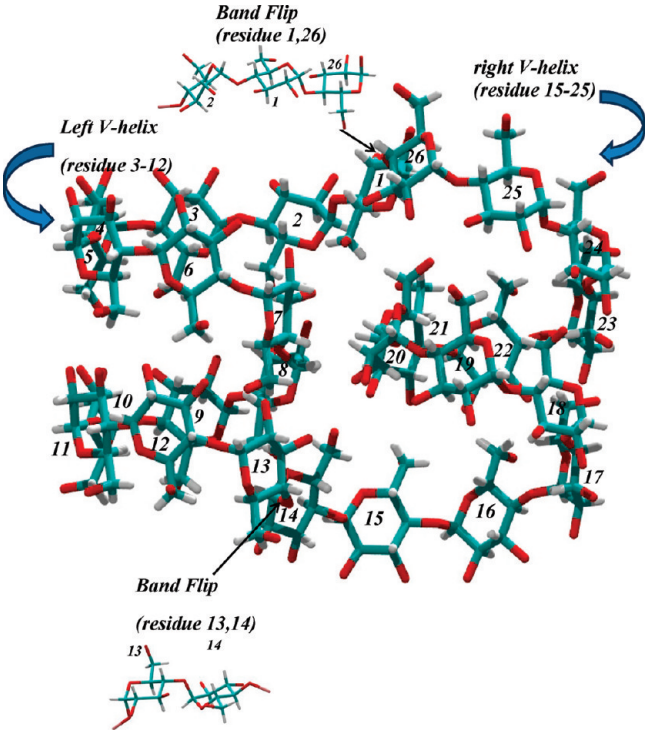

Figure 1. Stick figure of CA-26 with residue labels and "band-flip" residues. Hydrogen atoms on the exocyclic hydroxyls are not shown.

direct-polarized continuum model for solvent inclusion,[11] examined by the application of the B97D-PCM method. The self-consistent tight binding DFT, SCC-DFTB,[12] is a more semiempirical method but faster than the standard DFT methods.

Superimposing the heavy atoms of seven individual CA-26 X-ray crystal structures[1,4,5] (rsmd ≈ 0.88 Å; see Figure 2) shows that crystal packing forces play little role in the crystal conformations, and even the intercalation of small molecules into the helix fragments does not strongly change the secondary structure. In fact, taking all seven individual CA-26 structures and applying the rsmd test (see Table 2), one finds deviations between heavy atoms of the X-ray structures on the order of 0.3−1.5 Å. Upon examination of the structure denoted 1B, the structure utilized as a starting structure for this computational study, the rsmd values between other X-ray structures range from 0.62 to 1.04 Å. These results suggest that the molecule of CA-26 in the crystal form may be independently stable and serve as a critical test for different computational methodologies. Different water positions in the three crystal forms also appear to play only a small role in the overall conformations; however, ∼32−38 water molecules are found for each molecule in the three crystal structures. In this study, due to the size of the molecule, no explicit water molecules are included, although the application of solvent is tested using the B97D-PCM method. In three DFT calculations, but not the SCC-DFTB method, the reduced basis set is used, with different density functional variants.

COMPUTATIONAL DETAILS

All of the DFT studies reported used the starting structure heavy atoms taken from the X-ray crystal structure coordinates,[1] denoted 1B in Tables 1−4. Significant modifications in the X-ray structure were required prior to calculations. That is, in several residues, the orientation or position of the hydroxymethyl groups required refinement, a result of overlapping or double coordinates for some atom groups. After these preliminary adjustments, hydrogen atoms were added and positions refined using the semiempirical PM3 forces,[13] fixing the heavy atom positions. The hydroxymethyl groups were aligned as closely as possible to the positions found in the X-ray structure, with some minor exceptions, and the hydroxyl hydrogen atoms were optimized to point toward nearest-neighbor acceptor atoms. The Gaussian09 program was used throughout,[13] with calculations on a PQS[14] 16-processor, 3.0 GH computer, with extended memory. DFTr was applied to three DFT methods with basis sets of 6-31+G* on all atoms excepting carbon atoms, where 4-31G was used. Optimization was considered complete when the gradient difference reached 0.0025 au, the energy difference reached 10^{-5} Hartree, the displacement reached 0.01 Å, and no atom-specific variance was greater than 0.001 Å. These conditions for convergence differ by necessity from those developed for small molecules. The glycosidic bond dihedral angles ϕ_c and ψ_c were defined using the heavy atoms, $O5_n-C1_n-O4_{n-1}-C4_{n-1}$ and $C1_n-O4_{n-1}-C4_{n-1}-C5_{n-1}$, respectively. The hydroxymethyl groups are defined by three rotamers, gg, gt, and tg, where one defines these dihedral angles as $O5_n-C4_n-C5_n-O6_n$ = 60, −60, and 180°, respectively. The hydroxyl groups at the 2 and 3-positions are defined as either clockwise "c" or counterclockwise "r". The average number of gradient optimization cycles was ∼60−300 (300 for B3LYP), while the total machine time taken for an optimization cycle for the DFTr optimization was on the order of 25 000 CPU cycles. Results from optimization of other DFT methods are described, reoptimizing using the optimized DFTr-(B3LYP) structure as the starting structure. Other DFT methods include DFTr(B97D),[10] DFTr(B97D-PCM),[11] and SCC-DFTB.[12] Energies of the optimized structures cannot be compared with one another and are not included in the tables.

RESULTS AND DISCUSSION

Figure 2 shows the modified experimental starting X-ray and DFT structures as the rmsd fitted together, and in Figure 3 is shown a space-filling model of the optimized DFTr(B3LYP). Table 1 gives the conformational information including the hydroxymethyl and hydroxyl orientations for all seven X-ray structures, the starting structure derived from the X-ray coordinates, and the four DFT methods. Table 3 gives the rmsd values of the four DFT methods relative to the starting structure. In Table 4 is shown the rmsd between the optimized DFT structures and seven sets of X-ray coordinates. All originally *syn*-glucose residues retained the $^4C_1$ chair syn form after optimization. The band-flips and kinks between glucose residues were retained with little variation, and only a few glycosidic bond dihedral angles were twisted significantly from the crystal structure conformation. In Table 5 is shown the list of virtual distances $O4_n$-$O4_{n+1}$, glycosidic bond angles (Gly) $C1_n-O4_{n-1}-C4_{n-1}$, and glycosidic dihedral ϕ_c/ψ_c angles with the experimental starting values derived from the heavy atoms across the glycosidic bond. The bridge or band-flip regions are established as between residues 1 and 26 and residues 14 and 13. The dihedral angles at these sites are calculated to be very close to the experimental values for all DFT methods. On the other hand, optimization with the SCC-DFTB tight binding DFT resulted in glycosidic bond angles (Gly) smaller than those for the other DFT methods and smaller than the experimental values not only at the band-flip sites but generally throughout all of the linkages.

dx.doi.org/10.1021/jp208927v |J. Phys. Chem. B 2012, 116, 6618–6627

Table 1. Ring Conformation (RC), Hydroxymethyl Orientation (HM), and Exocyclic Hydroxyl Orientation (EH) for OH2 and OH3

	ring 1				ring 2				ring 3				ring 4				ring 5			
	RC	HM		EH	RC	HM		EH	RC	HM		EH	RC	HM		EH	RC	HM		EH
1A	4C1	gt			4C1	gg			4C1	gg			4C1	gg			4C1	gg		
1B	4C1	gt			4C1	gg			4C1	gt			4C1	gg			4C1	gg		
2A	4C1	gt			4C1	gg			4C1	gg			4C1	gg			4C1	gg		
2B	4C1	gt			4C1	gg			4C1	gt			4C1	gg			4C1	gg		
2C	4C1	gt			4C1	gg			4C1	gg			4C1	gg			4C1	gg		
3A	4C1	gt			4C1	gg			4C1	gg			4C1	gg			4C1	gg		
3B	4C1	gt			4C1	gg			4C1	gg			4C1	gg			4C1	gg		
B3LYP	4C1	gt	gauch−	rr	4C1	gg	gauch+	rr	4C1	gg	gauch+	cc	4C1	gg	gauch+	cc	4C1	gg	gauch+	rr
B97D-PCM	4C1	gt	gauch−	rr	4C1	gg	gauch+	rr	4C1	gg	gauch+	cc	4C1	gg	gauch+	cc	4C1	gg	gauch+	rr
B97D	4C1	gt	gauch−	rr	4C1	gg	gauch+	rr	4C1	gg	gauch+	cc	4C1	gg	gauch+	cc	4C1	gg	gauch+	rr
SCC-DFTB	4C1	gt	gauch−	rr	4C1	gg	gauch+	rr	4C1	gg	gauch+	cc	4C1	gg	gauch+	cc	4C1	gg	gauch+	rr
starting structure	4C1	gt	trans	rc	4C1	gg	gauch−	rc	4C1	gg	gauch−	rc	4C1	gg	gauch−	cc	4C1	gg	gauch+	rc

	ring 6				ring 7				ring 8				ring 9				ring 10			
	RC	HM		EH	RC	HM		EH	RC	HM		EH	RC	HM		EH	RC	HM		EH
1A	4C1	gg			4C1	gt			4C1	gg			4C1	gg			4C1	gt		
1B	4C1	gg			4C1	gt			4C1	gg			4C1	gg			4C1	gg		
2A	4C1	gg			4C1	gg			4C1	gg			4C1	gg			4C1	gg		
2B	4C1	gg			4C1	gg			4C1	gg			4C1	gg			4C1	gg		
2C	4C1	gg			4C1	gt			4C1	gt			4C1	gg			4C1	gt		
3A	4C1	gg			4C1	gt			4C1	gg			4C1	gt			4C1	gt		
3B	4C1	gg			4C1	gt			4C1	gg			4C1	gg			4C1	gg		
B3LYP	4C1	gg	gauch+	rr	4C1	gt	gauch−	rr	4C1	gg	gauch+	rc	4C1	gg	gauch+	cr	4C1	gg	gauch+	cc
B97D-PCM	4C1	gg	gauch+	rr	4C1	gt	gauch−	rr	4C1	gg	gauch+	rc	4C1	gg	gauch+	cr	4C1	gg	gauch+	cc
B97D	4C1	gg	gauch+	rr	4C1	gt	gauch−	rr	4C1	gg	gauch+	rc	4C1	gg	gauch+	cr	4C1	gg	gauch+	cc
SCC-DFTB	4C1	gg	gauch+	rr	4C1	gt	gauch−	rr	4C1	gg	gauch+	rc	4C1	gg	gauch+	cr	4C1	gg	gauch+	cc
starting structure	4C1	gg	gauch−	rc	4C1	gt	gauch−	rc	4C1	gg	gauch−	rc	4C1	gg	gauch+	rc	4C1	gg	gauch−	rc

	ring 11				ring 12				ring 13				ring 14				ring 15			
	RC	HM		EH	RC	HM		EH	RC	HM		EH	RC	HM		EH	RC	HM		EH
1A	4C1	gg			4C1	gg			4C1	gg			4C1	gt			4C1	gg		
1B	4C1	gt			4C1	gt			4C1	gt			4C1	gt			4C1	gg		
2A	4C1	gg			4C1	gg			4C1	gg			4C1	gt			4C1	gg		
2B	4C1	gg			4C1	gg			4C1	gg			4C1	gt			4C1	gg		
2C	4C1	gg			4C1	gg			4C1	gt			4C1	gt			4C1	gg		
3A	4C1	gt			4C1	gt			4C1	gt			4C1	gt			4C1	gg		
3B	4C1	gg			4C1	gg			4C1	gt			4C1	gt			4C1	gg		
B3LYP	4C1	gg	gauch+	cc	4C1	gg	gauch+	cr	4C1	gg	gauch+	rc	4C1	gt	trans	cc	4C1	gg	trans	cc
B97D-PCM	4C1	gg	gauch+	cc	4C1	gg	gauch+	cr	4C1	gg	gauch+	rc	4C1	gt	trans	cc	4C1	gg	trans	cc
B97D	4C1	gg	gauch+	cc	4C1	gg	gauch+	cr	4C1	gg	gauch+	rc	4C1	gt	gauch+	cc	4C1	gg	trans	cc
SCC-DFTB	4C1	gg	gauch+	cc	4C1	gg	gauch+	cr	4C1	gg	gauch+	rc	4C1	gt	trans	cc	4C1	gg	trans	cc
starting structure	4C1	gg	gauch−	rc	4C1	gg	gauch−	rc	4C1	gg	gauch−	rc	4C1	gt	trans	rc	4C1	gg	gauch−	rc

	ring 16				ring 17				ring 18				ring 19				ring 20			
	RC	HM		EH	RC	HM		EH	RC	HM		EH	RC	HM		EH	RC	HM		EH
1A	4C1	gt			4C1	gg	trans		4C1	gg			4C1	gg			4C1	gt		
1B	4C1	gg			4C1	gg	trans		4C1	gg			4C1	gg			4C1	gt		
2A	4C1	gg			4C1	gg	gauch−		4C1	gg			4C1	gg			4C1	gt		
2B	4C1	gg			4C1	gg	gauch−		4C1	gg			4C1	gg			4C1	gg		

dx.doi.org/10.1021/jp208927v |J. Phys. Chem. B 2012, 116, 6618–6627

Table 1. Continued

	ring 16				ring 17				ring 18				ring 19				ring 20			
	RC	HM		EH	RC	HM		EH	RC	HM		EH	RC	HM		EH	RC	HM		EH
2C	4C1	gg			4C1	gg	gauch−		4C1	gg			4C1	gg			4C1	gt		
3A	4C1	gg			4C1	gg	gauch−		4C1	gg			4C1	gg			4C1	gt		
3B	4C1	gt			4C1	gg	gauch−		4C1	gg			4C1	gg			4C1	gt		
B3LYP	4C1	gg	gauch−	cc	4C1	gt	trans	cr	4C1	gg	gauch+	rr	4C1	gg	gauch+	rc	4C1	gt	gauch−	cc
B97D-PCM	4C1	gg	gauch−	cc	4C1	gt	trans	cr	4C1	gg	gauch+	rr	4C1	gg	gauch+	rc	4C1	gt	gauch−	cc
B97D	4C1	gg	gauch−	cc	4C1	gt	gauch−	cr	4C1	gg	gauch+	rr	4C1	gg	gauch+	rc	4C1	gt	gauch−	cc
SCC-DFTB	4C1	gg	gauch−	cc	4C1	gt	trans	cr	4C1	gg	gauch+	rr	4C1	gg	gauch+	rc	4C1	gt	gauch−	cc
starting structure	4C1	gg	gauch−	rc	4C1	gt	gauch+	rc	4C1	gg	gauch−	rc	4C1	gg	gauch−	rc	4C1	gt	gauch−	rc

	ring 21				ring 22				ring 23				ring 24				ring 25			
	RC	HM		EH	RC	HM		EH	RC	HM		EH	RC	HM		EH	RC	HM		EH
1A	4C1	gg			4C1	gt			4C1	gt			4C1	gt			4C1	gt		
1B	4C1	gg			4C1	gg			4C1	gg			4C1	gt			4C1	gg		
2A	4C1	gg			4C1	gg			4C1	gg			4C1	gg			4C1	gg		
2B	4C1	gg			4C1	gg			4C1	gg			4C1	gg			4C1	gg		
2C	4C1	gg			4C1	gt			4C1	gt			4C1	gt			4C1	gg		
3A	4C1	gg			4C1	gt			4C1	gt			4C1	gt			4C1	gt		
3B	4C1	gg			4C1	gt			4C1	gg			4C1	gg			4C1	gg		
B3LYP	4C1	gg	trans	cc	4C1	gg	gauch+	cr	4C1	gg	gauch+	rc	4C1	gg	gauch+	rr	4C1	gg	gauch+	rr
B97D-PCM	4C1	gg	trans	cc	4C1	gg	gauch+	cr	4C1	gg	gauch+	rc	4C1	gg	gauch+	rr	4C1	gg	gauch+	rr
B97D	4C1	gg	trans	cc	4C1	gg	gauch+	cr	4C1	gg	gauch+	rc	4C1	gg	gauch+	rr	4C1	gg	gauch+	rr
SCC-DFTB	4C1	gg	trans	cc	4C1	gg	gauch+	cr	4C1	gg	gauch+	rc	4C1	gg	gauch+	rr	4C1	gg	gauch+	rr
starting structure	4C1	gg	gauch−	cc	4C1	gg	gauch+	rc	4C1	gg	gauch−	rc	4C1	gg	gauch−	rr	4C1	gg	gauch−	rc

	ring 26		
	RC	HM	EH
1A	4C1	gg	
1B	4C1	gg	
2A	4C1	gg	
2B	4C1	gg	
2C	4C1	gt	
3A	4C1	gt	
3B	4C1	gt	
B3LYP	4C1	gg	gauch+ rr
B97D-PCM	4C1	gg	gauch+ rr
B97D	4C1	gg	gauch+ rr
SCC-DFTB	4C1	gg	gauch+ rr
starting structure	4C1	gg	gauch− cc

The ring geometry for all of the DFT structures was quite good, as described by the Vd ($O4_n \cdots O4_{n-1}$) distances and the Cremer−Pople[15] parameters given in Table 6.

Of interest is the repeat distance obtained from the V-helical segments of CA-26 when compared to the crystal structure of other amylose structures. For example, in B-amylose, the pitch value of 10.57 Å[16] is found. However, V-amylose is found experimentally as left-handed single helix chains of six glucose residues per turn with a 7.91−8.17 Å pitch height.[17−21] From the X-ray structure of CA-26, the pitch height is ∼7.9 Å, with the helices oriented antiparallel to one another, in excellent agreement with pitch values of the V-helix of linear molecules. The equivalent DFT (Rd in Table 6 and individual helices in Table 7) values obtained are 7.83−7.99 Å, taken as an average of six residue repeats over each helix. In Table 7, the V-helix segment pitch heights are individually presented, varying from the smallest value, 7.52 Å for structure 1A, in segment 15−21, to 8.76 Å for 2B, in segment 3−9. The DFT values cluster around 7.9 Å, with the smallest value of 7.1 Å at the 16−22 residue fragment for B97D to the largest values of 8.6 Å for B3LYP for helical segment 17−23.

The independent stability of the helical segments was tested by isolating the V-helix segment from the previous optimized CA-26 and reoptimizing using the B97D-PCM method. It is an interesting question as to the V-helix stability, and although optimization only proceeds in the local energy well previously

dx.doi.org/10.1021/jp208927v |J. Phys. Chem. B 2012, 116, 6618–6627

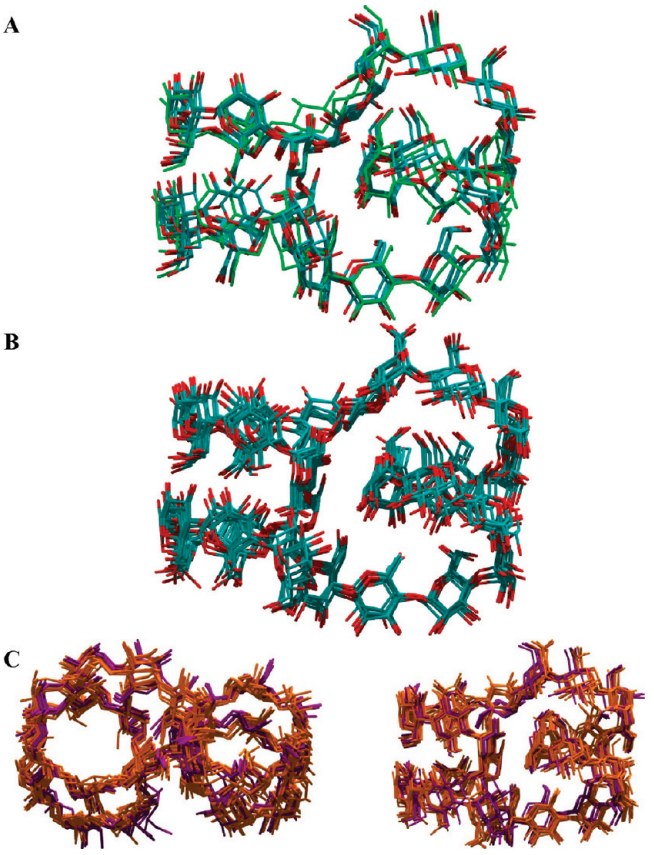

Figure 2. Stick figures of CA-26 shown without hydrogen atoms. (A) DFT (B3LYP, B97D, B97D-PCM, SCC-DFTB) and the starting structure 1B (green). (B) Seven X-ray structures from refs 1, 4, and 5. (C) DFT methods (orange) and seven X-ray structures (purple) in two different views.

Table 2. Calculated RMSD Deviations between X-ray Structures

	X-ray structures[a]					
	1A[b]	1B	2A[c]	2B	2C	3A[d]
1A	0.00					
1B	0.94	0.00				
2A	1.02	0.79	0.00			
2B	1.21	0.79	0.62	0.00		
2C	1.44	1.02	0.71	0.84	0.00	
3A	1.46	1.04	0.75	0.87	0.28	0.00
3B	0.78	0.62	0.82	0.78	1.16	1.20

[a] In the case of paired structures in a unit cell, each individual structure was extracted. [b] Reference 1. [c] Reference 4. [d] Reference 5.

established, it remains of interest to see how different the V-helix is when it is not constrained within the cyclic molecule. The rmsd of the isolated V-helix relative to the starting structure was found to be 0.22; see Figure 4. One can conclude from this that the V-helix is relatively stable by itself and does not unfold to a new conformational state during optimization.

Our interest in studying different DFTr methods is of particular significance in that it has been suggested that one should include dispersion in the study of medium size organic molecules. CA-26 is an excellent test case because one could expect to find deviations in the soft geometric parameters of this relatively large molecule when including dispersion terms in the energy during optimization (see Tables 3 and 4). Analyses of the

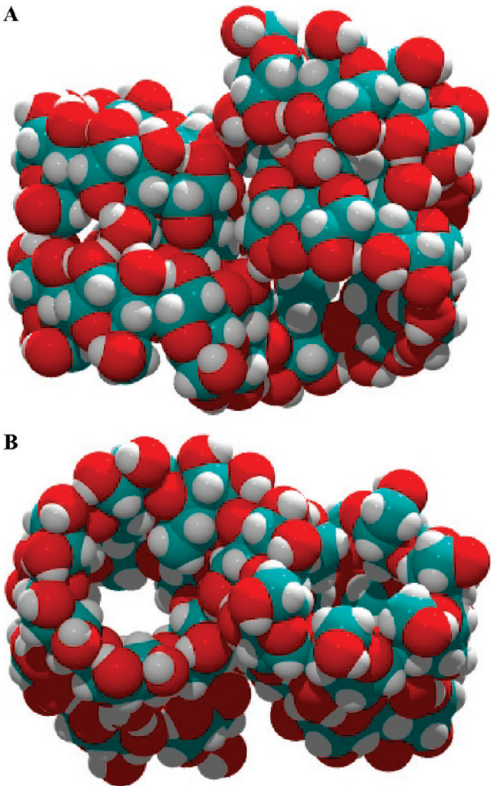

Figure 3. Space-filling figures of CA-26 of the optimized DFTr (B3LYP) vacuum structure. (A) side view; (B) top view.

Table 3. Calculated RMSD Deviations between the DFT Methods and Starting Structure[a]

	SCC-DTFB	B3LYP	B97D	B97D-PCM
SCC-DTFB	0.00			
B3LYP	0.40	0.00		
B97D	0.75	0.71	0.00	
B97D-PCM	0.35	0.17	0.62	0.00
starting structure	0.94	0.90	1.38	0.95

[a] Reference 1, with slightly modified structural parameters to obtain good starting coordinates for the DFT optimizations.

Table 4. Calculated RMSD Deviations between DFT Methods and X-ray Structures

	X-ray structures[a]						
	1A	1B	2A	2B	2C	3A	3B
SCC-DFTB	1.16	0.91	0.90	0.91	1.06	1.09	1.06
B3LYP	1.20	0.88	0.77	0.79	0.86	0.92	1.05
B97D	1.59	1.37	1.12	1.14	1.07	1.06	1.53
B97D-PCM	1.22	0.91	0.77	0.80	0.86	0.92	1.08

[a] References 1, 4, and 5.

dx.doi.org/10.1021/jp208927v |J. Phys. Chem. B 2012, 116, 6618–6627

Table 5. ϕ_C/ψ_C Torsional Angles, Glycosidic Bond Angle $C1_n-O4_{n-1}-C4_{n-1}$ (Gly), and Virtual Distance $O4_n-O4_{n-1}$ (Vd)

	bridge 1−26				bridge 2−1				bridge 3−2				bridge 4−3			
	ϕ_C	ψ_C	Gly	Vd	ϕ_C	ψ_C	Gly	Vd	ϕ_C	ψ_C	Gly	Vd	ϕ_C	ψ_C	Gly	Vd
1A	87.8	−46.3	117.7	4.58	100.8	112.3	117.3	4.79	103.5	119.5	116.6	4.52	104.7	120.1	116.7	4.17
1B	88.0	−49.6	116.7	4.61	105.1	121.3	118.4	4.62	92.2	107.7	115.7	4.53	101.3	123.7	118.5	4.36
2A	88.0	−53.6	116.7	4.64	101.8	114.4	115.3	4.60	103.2	106.7	115.7	4.47	108.3	120.7	118.1	4.27
2B	87.8	−49.2	118.2	4.43	106.9	115.7	117.2	4.47	82.1	90.0	114.9	4.49	129.9	133.9	117.7	4.28
2C	88.1	−51.2	117.0	4.56	100.5	118.4	117.6	4.64	103.2	106.9	116.4	4.43	106.3	112.7	118.2	4.31
3A	84.9	−49.0	117.8	4.55	98.0	119.0	117.5	4.60	101.9	106.9	116.0	4.43	106.3	113.2	117.6	4.34
3B	88.6	−38.4	117.9	4.47	108.0	86.8	117.5	4.70	101.6	114.6	116.1	4.50	114.6	124.4	118.6	4.31
B3LYP	85.0	−35.3	116.9	4.66	97.5	142.4	117.0	4.67	76.2	92.3	113.6	4.52	108.2	113.3	117.8	4.45
B97D-PCM	86.0	−38.5	115.3	4.62	98.8	141.7	116.8	4.62	74.2	95.6	112.4	4.55	105.0	116.4	117.1	4.40
B97D	85.1	−38.0	115.3	4.61	93.1	145.5	116.4	4.61	75.8	94.0	112.8	4.50	104.8	114.3	116.8	4.47
SCC-DFTB	85.5	−39.6	114.4	4.61	105.3	137.7	114.2	4.52	72.1	85.5	110.3	4.45	108.2	108.7	114.3	4.39
starting structure	89.8	−47.7	117.2	4.49	102.5	112.5	116.8	4.71	99.9	116.0	114.7	4.52	107.0	120.2	117.9	4.20

	bridge 5−4				bridge 6−5				bridge 7−6				bridge 8−7			
	ϕ_C	ψ_C	Gly	Vd	ϕ_C	ψ_C	Gly	Vd	ϕ_C	ψ_C	Gly	Vd	ϕ_C	ψ_C	Gly	Vd
1A	101.6	113.1	120.1	4.18	102.0	109.7	117.3	4.35	105.9	120.4	118.2	4.22	108.4	106.6	118.2	4.31
1B	97.2	115.2	117.7	4.30	100.2	116.6	118.3	4.21	102.1	110.7	120.0	4.32	104.0	116.4	118.1	4.36
2A	104.1	118.9	117.9	4.29	95.1	124.7	118.5	4.25	98.6	118.3	118.7	4.37	103.8	114.9	117.7	4.25
2B	103.2	119.5	117.3	4.18	92.4	114.9	118.0	4.26	100.9	124.5	117.4	4.37	101.8	112.3	117.0	4.20
2C	104.8	118.4	118.2	4.24	104.5	103.8	120.1	4.21	109.0	116.7	119.2	4.38	103.4	117.7	119.0	4.27
3A	104.8	115.7	119.4	4.24	107.3	104.1	119.6	4.20	108.5	117.4	119.2	4.37	103.0	115.1	118.2	4.25
3B	106.9	117.1	118.0	4.19	96.5	110.6	118.9	4.37	105.9	120.7	119.3	4.22	106.4	108.3	118.5	4.33
B3LYP	107.2	115.9	117.8	4.33	104.6	121.9	119.2	4.33	97.9	120.8	119.0	4.35	105.8	113.3	117.8	4.40
B97D-PCM	103.8	117.5	117.2	4.35	105.1	118.6	118.2	4.33	100.4	119.0	118.4	4.27	105.7	114.3	116.9	4.37
B97D	105.4	121.9	117.3	4.30	105.5	112.2	118.2	4.24	98.8	124.5	118.5	4.38	108.2	110.8	117.0	4.34
SCC-DFTB	110.1	118.3	114.8	4.21	110.0	98.5	114.5	4.24	105.7	120.6	115.6	4.24	109.7	103.3	114.4	4.27
starting structure	107.2	114.8	119.1	4.14	97.9	107.4	119.4	4.33	105.6	126.2	119.6	4.24	106.2	109.1	117.2	4.34

	bridge 9−8				bridge 10−9				bridge 11−10				bridge 12−11			
	ϕ_C	ψ_C	Gly	Vd	ϕ_C	ψ_C	Gly	Vd	ϕ_C	ψ_C	Gly	Vd	ϕ_C	ψ_C	Gly	Vd
1A	108.6	114.8	118.6	4.17	102.7	123.1	118.9	4.26	102.9	120.8	118.7	4.41	104.4	117.0	117.9	4.44
1B	103.9	110.8	116.8	4.18	113.8	110.9	120.3	4.33	102.4	119.7	119.2	4.37	109.9	125.4	119.5	4.41
2A	106.2	116.0	118.7	4.19	102.0	123.8	118.7	4.29	99.8	119.6	117.6	4.31	99.2	123.0	117.7	4.41
2B	110.0	100.6	118.1	4.17	111.1	128.6	118.8	4.28	102.5	116.9	117.9	4.28	103.8	119.5	118.4	4.38
2C	104.3	116.3	119.6	4.29	103.0	115.8	119.3	4.29	98.3	119.7	119.7	4.28	105.0	133.3	119.1	4.48
3A	107.2	114.7	119.8	4.26	104.8	116.3	118.8	4.31	102.9	119.7	117.4	4.25	103.2	128.0	119.0	4.45
3B	105.8	113.4	118.7	4.25	109.4	110.1	119.3	4.26	107.4	122.3	120.5	4.31	103.9	113.1	118.3	4.43
B3LYP	106.3	120.5	118.1	4.22	92.2	122.3	117.4	4.40	96.1	121.8	117.2	4.60	108.4	109.8	117.1	4.45
B97D-PCM	103.8	121.0	117.3	4.21	87.4	125.7	117.2	4.43	103.4	116.9	116.6	4.47	104.8	116.0	116.6	4.43
B97D	102.8	120.8	118.0	4.07	89.8	123.8	117.3	4.46	109.1	121.5	116.6	4.54	105.0	117.3	116.8	4.38
SCC-DFTB	108.9	115.4	114.9	4.09	94.0	119.9	114.4	4.38	109.2	116.6	114.3	4.46	106.3	106.4	113.9	4.35
starting structure	103.7	114.4	118.5	4.24	101.8	117.5	121.3	4.25	103.6	117.1	119.6	4.37	104.8	114.7	116.3	4.40

	bridge 13−12				bridge 14−13				bridge 15−14				bridge 16−15			
	ϕ_C	ψ_C	Gly	Vd	ϕ_C	ψ_C	Gly	Vd	ϕ_C	ψ_C	Gly	Vd	ϕ_C	ψ_C	Gly	Vd
1A	99.1	111.5	118.3	4.50	87.0	−52.4	118.4	4.70	115.4	131.3	117.5	4.68	92.2	100.7	114.4	4.54
1B	93.5	106.4	118.4	4.52	90.6	−46.0	118.1	4.55	102.2	98.1	115.8	4.70	112.1	129.5	116.7	4.43
2A	104.0	131.7	117.4	4.50	87.6	−51.9	117.8	4.43	102.6	110.9	116.1	4.74	98.5	109.0	114.0	4.48
2B	102.4	131.0	116.2	4.51	88.0	−52.9	117.0	4.38	97.8	118.4	117.6	4.62	92.0	105.9	115.4	4.67
2C	92.7	110.7	115.1	4.67	88.1	−51.2	117.1	4.56	100.5	118.4	117.6	4.64	103.1	106.9	116.4	4.43
3A	100.7	110.4	117.1	4.70	84.9	−49.0	117.8	4.55	97.9	119.0	117.5	4.60	101.9	106.9	116.0	4.43

dx.doi.org/10.1021/jp208927v |J. Phys. Chem. B 2012, 116, 6618–6627

Table 5. Continued

	bridge 13−12				bridge 14−13				bridge 15−14				bridge 16−15			
	ϕ_C	ψ_C	Gly	Vd	ϕ_C	ψ_C	Gly	Vd	ϕ_C	ψ_C	Gly	Vd	ϕ_C	ψ_C	Gly	Vd
3B	101.1	121.0	117.9	4.55	89.5	−42.9	117.9	4.54	101.4	110.4	115.2	4.76	94.4	103.0	114.5	4.53
B3LYP	107.0	104.6	117.4	4.59	88.6	−47.1	117.0	4.65	101.7	126.6	116.1	4.60	110.8	116.3	118.6	4.53
B97D-PCM	103.3	103.2	115.8	4.54	88.1	−49.7	115.4	4.62	101.4	127.7	115.8	4.58	108.4	118.2	117.7	4.51
B97D	103.2	96.9	116.4	4.41	85.5	−49.0	115.9	4.49	99.9	139.8	116.6	4.46	108.0	119.9	118.4	4.46
SCC-DFTB	108.6	95.9	114.0	4.37	88.8	−51.1	114.3	4.55	107.6	126.5	113.7	4.48	110.1	114.6	114.9	4.42
starting structure	102.3	109.3	115.4	4.51	87.8	−50.5	117.1	4.59	105.8	123.4	116.9	4.58	100.9	99.8	114.5	4.57
	bridge 17−16				bridge 18−17				bridge 19−18				bridge 20−19			
	ϕ_C	ψ_C	Gly	Vd	ϕ_C	ψ_C	Gly	Vd	ϕ_C	ψ_C	Gly	Vd	ϕ_C	ψ_C	Gly	Vd
1A	103.7	122.3	119.4	4.25	110.7	110.2	119.7	4.13	100.1	106.9	117.2	4.37	105.8	119.1	118.1	4.22
1B	98.3	114.6	118.7	4.42	105.8	115.6	120.5	4.23	103.1	115.1	118.6	4.31	101.5	117.6	119.8	4.32
2A	106.3	123.9	118.2	4.17	105.4	118.5	118.3	4.26	97.8	115.9	116.5	4.33	104.7	118.3	118.3	4.18
2B	111.6	124.4	118.9	4.23	109.8	114.0	118.0	4.11	89.9	132.0	118.0	4.41	100.5	122.5	115.7	4.36
2C	106.3	112.8	118.2	4.32	104.8	118.4	118.3	4.24	104.6	103.8	120.1	4.20	109.0	116.8	119.2	4.38
3A	106.3	113.2	117.6	4.34	104.9	115.7	119.4	4.24	107.2	104.2	119.6	4.20	108.5	117.5	119.1	4.37
3B	108.5	122.6	118.8	4.22	111.2	102.2	119.2	4.30	101.2	116.9	119.1	4.29	104.3	120.0	120.2	4.33
B3LYP	96.5	100.1	115.1	4.34	107.5	134.4	120.5	4.21	99.7	108.8	118.4	4.31	103.3	106.8	117.3	4.44
B97D-PCM	96.9	100.9	114.4	4.32	108.1	130.5	119.7	4.20	100.3	113.4	117.6	4.31	101.2	108.2	116.7	4.41
B97D	96.3	101.3	114.3	4.39	105.7	131.8	118.9	4.25	94.9	121.3	118.2	4.23	104.3	98.3	116.6	4.45
SCC-DFTB	97.6	95.3	112.2	4.29	109.2	128.1	116.1	4.09	109.4	92.1	114.3	4.20	108.9	104.6	114.6	4.36
starting structure	108.0	114.7	116.6	4.30	111.0	127.3	121.3	4.04	95.8	105.9	116.2	4.40	103.3	116.9	117.4	4.20
	bridge 21−20				bridge 22−21				bridge 23−22				bridge 24−23			
	ϕ_C	ψ_C	Gly	Vd	ϕ_C	ψ_C	Gly	Vd	ϕ_C	ψ_C	Gly	Vd	ϕ_C	ψ_C	Gly	Vd
1A	112.0	105.9	118.8	4.37	108.8	109.3	118.7	4.11	106.2	121.7	120.4	4.26	105.7	123.2	119.2	4.43
1B	104.0	113.2	118.7	4.26	105.0	109.8	118.2	4.22	105.7	113.6	119.0	4.31	103.0	120.2	119.8	4.27
2A	101.3	114.6	116.8	4.31	108.4	120.3	116.3	4.26	99.9	119.4	117.5	4.21	99.3	122.2	117.5	4.29
2B	104.7	112.7	116.9	4.17	100.8	114.9	117.9	4.33	105.5	123.3	118.0	4.25	100.7	124.5	118.9	4.26
2C	103.4	117.7	119.1	4.27	104.3	116.4	119.6	4.29	103.0	115.8	119.4	4.29	98.4	119.7	119.7	4.28
3A	102.9	115.0	118.3	4.25	107.2	114.7	119.7	4.26	104.8	116.3	118.8	4.31	102.9	119.7	117.4	4.25
3B	105.7	112.8	118.7	4.40	98.2	115.5	117.9	4.22	106.0	111.0	119.5	4.24	105.5	123.9	119.2	4.47
B3LYP	111.9	118.5	119.4	4.33	108.3	103.6	118.7	4.26	109.9	119.0	119.4	4.33	108.2	125.8	118.3	4.42
B97D-PCM	112.0	118.9	118.6	4.26	106.1	104.0	117.3	4.27	109.0	120.0	118.6	4.29	103.4	125.3	117.4	4.41
B97D	114.6	126.6	118.5	4.25	104.6	106.8	117.5	4.21	109.0	118.2	118.5	4.32	101.4	128.3	117.3	4.40
SCC-DFTB	113.5	116.8	115.5	4.24	109.9	97.5	114.5	4.17	114.0	112.5	115.8	4.22	108.9	126.0	114.9	4.36
starting structure	108.2	114.0	118.7	4.32	104.8	102.5	117.6	4.15	112.4	112.0	120.8	4.23	110.6	126.7	118.7	4.49

	bridge 25−24			
	ϕ_C	ψ_C	Gly	Vd
1A	101.9	112.6	118.5	4.39
1B	109.0	121.9	118.4	4.41
2A	100.3	125.0	117.4	4.45
2B	101.0	107.4	116.7	4.38
2C	104.9	133.3	119.0	4.48
3A	103.2	128.1	119.0	4.45
3B	99.3	113.1	116.9	4.35
B3LYP	101.3	118.0	117.1	4.53
B97D	102.7	118.6	116.4	4.51
B97D-PCM	100.6	121.8	116.3	4.53
SCC-DFTB	103.2	111.2	113.6	4.46
starting structure	103.4	108.8	117.6	4.37

dx.doi.org/10.1021/jp208927v |J. Phys. Chem. B 2012, 116, 6618–6627

Table 6. Averaged Geometric Data of the V-Helical Segments of DP26, Torsional Angles ϕ_C and ψ_C, Glycosidic Bond Angle (Gly) $C1_n-O4_{n-1}-C4_{n-1}$, Virtual Distance (Vd) $O4_n-O4_{n-1}$, Virtual Angle (Va) $O4_n-O4_{n-1}-O4_{n-2}$, Inter-Glucose Hydrogen Bond Distance (Hb) $O3_n-O2_{n-1}$, V-Helix Repeat Distance (Rd) $O5_n-O5_{n+6}$, Cremer−Pople Puckering Amplitude (Q), and Angle Theta (θ)

	torsion							Cremer−Pople	
	ϕ_C	ψ_C	Gly	Vd	Va	Hb	Rd	Q	θ
1A	104.7	115.3	118.2	4.35	126.3	2.86	7.91	0.547	5.24
1B	103.3	115.4	118.5	4.36	127.9	2.90	7.96	0.545	4.16
2A	102.2	118.7	117.3	4.34	126.6	2.87	7.88	0.571	3.87
2B	102.7	117.7	117.4	4.33	126.8	2.95	7.95	0.568	5.03
2C	103.4	116.1	118.6	4.36	127.7	2.84	7.99	0.555	4.48
3A	104.2	115.3	118.3	4.35	127.8	2.80	8.02	0.566	2.87
3B	104.5	113.6	118.3	4.37	127.3	2.86	8.03	0.549	4.86
B3LYP	102.9	116.4	117.7	4.42	127.4	3.01	7.99	0.560	5.27
B97D-PCM	102.0	117.0	117.0	4.39	127.2	2.96	7.85	0.574	4.13
B97D	101.8	118.2	117.1	4.38	127.0	3.00	7.83	0.577	4.86
DFTB	106.1	110.9	114.3	4.32	127.2	2.94	7.91	0.590	5.71
starting structure	104.7	114.4	117.9	4.34	127.2	2.84	8.00	0.552	5.18

Table 7. V-Helix Repeat Distances $O5_n-O5_{n+6}$ (Left V-Helix Ring 3−12 and Right V-Helix Ring 15−25)

	residue number								
	3−9	4−10	5−11	6−12	15−21	16−22	17−23	18−24	19−25
1A	7.89	7.77	7.92	7.98	7.52	8.36	8.13	7.78	7.83
1B	8.19	8.00	7.77	7.94	8.24	7.77	7.94	7.83	7.95
2A	7.99	7.79	7.62	7.70	7.54	8.50	8.12	7.74	7.90
2B	8.76	7.93	7.69	7.86	7.48	7.90	7.70	8.20	8.02
2C	8.00	7.89	7.74	8.35	7.92	8.00	7.89	7.74	8.35
3A	8.09	7.93	7.83	8.30	7.91	8.09	7.93	7.83	8.30
3B	8.45	7.97	7.98	7.99	7.64	8.13	7.86	8.23	8.05
B3LYP	8.05	7.91	8.10	7.94	8.04	7.44	8.64	8.06	7.73
B97D-PCM	7.88	7.87	8.15	7.73	7.96	7.29	8.36	7.82	7.63
B97D	7.91	8.07	8.30	7.80	7.99	7.11	8.09	7.72	7.50
DFTB	7.90	8.14	8.18	7.83	7.91	7.23	8.47	7.94	7.64
starting structure	8.00	7.71	7.77	8.26	7.80	8.28	8.59	7.81	7.77

rmsd results do not in themselves confirm that dispersion plays a significant role in the conformation of the minimum-energy structure, even though there are numerous long-range interactions in the CA-26 molecule that apply attractive forces on the structure. The observation that the rmsds of the B97D with and without solvent (0.91 versus 1.37 Å, respectively, in Table 4) are both larger than the B3LYP value (0.88 Å), suggests that including dispersion does not, in this case, improve the fit to the experimental structure, even though addition of implicit solvent with dispersion does improve the fit to the experimental data relative to the dispersion-corrected-only fit. The tight binding, SCC-DFTB, rmsd results (0.94 Å in Table 3) approach those from the B3LYP optimization, which provides some optimism for use of this very rapid calculation method for further study of large carbohydrate molecules. However, as noted later, there are some questions about using the version used here for carbohydrates.

In an attempt to understand the stability of the CA-26 molecule and the dimer in the crystalline unit cell, the dipole moments of the complete molecule and individually its two helical segments were calculated. The two helical segments of CA-26 were superimposed and atoms cut away until the identical helical fragments remained with the identical number and types of atoms. The two helical segments were valence-balanced by adding hydrogen atoms on the terminal atoms. The energies and dipole moments were calculated by several different DFT methods to check, and the results were consistent, that is, no one DFT method gave different dipole values than any other method. The results were interesting in that the magnitude of the dipole moments in vacuo were in the range of 16−18 D, not directed along the helical axis but rather tilted off of the ideal helical axis, thus not completely balanced in opposite directions. The complete CA-26 molecule produced an in vacuo dipole moment of ∼29 D, approximately twice the individual dipole moments of the helical segments. A dipole of this magnitude would be a source of energetic molecular orientation in the crystal and is most probably neutralized by the dimer formation of the second molecule in the crystal unit cell. Although somewhat surprising in magnitude, it is also possible that the water molecules (missing in this work) in the crystal structure further act to suppress the overall dipole moment. In particular, the water

dx.doi.org/10.1021/jp208927v |J. Phys. Chem. B 2012, 116, 6618–6627

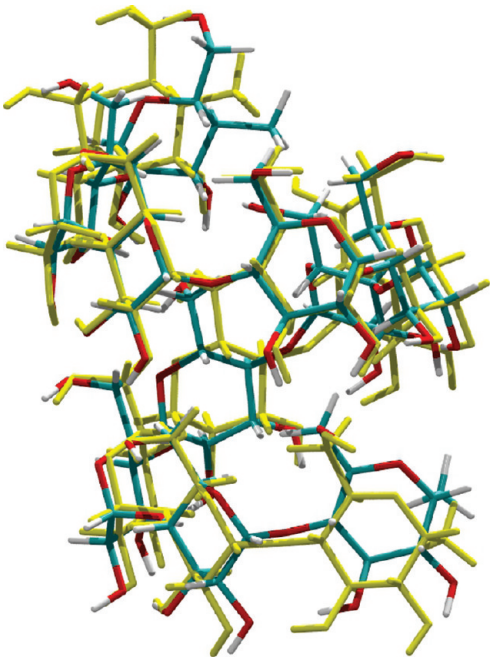

Figure 4. Stick figure of the left V-helix of CA-26 showing the difference between the DFTr (B97D-PCM) optimizations of the V-helix in the CA-26 and the unconstrained V-helix (solid yellow lines).

molecules located in the core of the two helical segments may orientate such that they balance out some of the molecular dipole moments in those segments. The optimized DFTr(B97D-PCM) helical fragment showed some variation from the complete fragment but primarily in the terminal glucose residue rotating slightly to complete a triad of hydrogen bonds. In the complete CA-26 molecule, this movement was prevented by the continuation to the other helical segment.

It is of interest to examine the molecular conformation relative to the glycosidic dihedral angles, ϕ_c/ψ_c. The immediate observation is that the calculated dihedral angles are very close to the X-ray values (Table 5). However, by summing and averaging the dihedral angles, one may find trends in the values that do not appear in any individual set of dihedrals (see Table 6). For example, the AMB06C potentials[6] showed that both ϕ_c and ψ_c were, on average, smaller than the experimental values by 4−5°.[6] With the exception of the SCC-DFTB results, there appear to be no significant deviations from experiment in the three other DFT methods. Comparing the average values of several parameters to the X-ray average values shows the following trends. The average deviations of the dihedral angles, ϕ_c/ψ_c, for the DFT optimized structures given in Table 6 shows that deviations of the DFT results from the average X-ray values are on the order of 1−2°, with the largest deviations being from the SCC-DFTB results. Similarly for the glycosidic angle (Gly), we find that the DFT results are again, with the exception of the SCC-DFTB result, very close to the X-ray structures. The comparison of averaged parameters is found to be excellent throughout the DFT results in Table 6, but again, the tight binding DFTB method has significant deviations. Another internal coordinate examined, but not in the tables, is the O5—C1—O4 angle around the anomeric carbon atom for all 26 residues. The average value for the SCC-DFTB method was ∼111°, while all other experimental and DFT values were ∼109° with a ∼1° deviation.

CONCLUSION

Introduction of the reduced basis set DFTr method has allowed a high-level electronic computational study of a large carbohydrate using relatively small computing facilities. It would have been of interest to carry out room-temperature molecular dynamics on these structures; unfortunately, that ability would have required computer facilities unavailable to the authors at this time. Comparing the optimized conformations (0° K) to X-ray structures whose data were taken at temperatures much above 0 K is not optimal, but as described, there was much to learn from these studies.

Although the reduced basis set method, DFTr, is specific for application to carbohydrates because of the geometry of the rings and the relative framework of the carbon atoms in the six-member ring, this study places a high-quality DFTr methodology into the toolbox of methods for study of modestly large fragments of carbohydrates in different configurations and environments.

From this study, it is apparent that prediction of V-helix, band-flip, and kink conformations are well within the ability of DFTr methods to accurately describe structural features of large carbohydrate molecules. The rmsd of the calculated optimized structures to the X-ray structures is on the order of the values found between the seven different X-ray structures, even those structures in which small molecules are intercalated into the V-helical segments.[1−5] The fact that one can even optimize these structures with DFT methodology is remarkable, and the high quality of the results gives us confidence that one can use DFTr methods to discover the stabilization and hydration factors that govern other modestly sized amylose- and cellulose-based carbohydrate fragments. The exception to the high-quality results of the DFT methods is the tight binding SCC-DFTB method, where considerable deviations from the experimental structures appear. Although it is useful to have this method available for large carbohydrates because of its speed, without further improvement, it would not be strongly recommended except to create large molecule conformations.

AUTHOR INFORMATION

Corresponding Author

*Tel. +1 309 681 6362. E-mail: frank.momany@ars.usda.gov.

REFERENCES

(1) Gessler, K.; Uson, I.; Takaha, T.; Krauss, N.; Smith, S. M.; Okada, S.; Sheldrick, G.; Saenger, W. *Proc. Natl. Acad. Sci. U.S.A.* **1999**, *96*, 4246–4251.

(2) Jacob, J.; Gessler, K.; Hoffman, D.; Sanbe, H.; Koizumi, K.; Smith, S. M.; Takaha, T.; Saenger, W. *Angew. Chem., Int. Ed.* **1998**, *37*, 605–609.

(3) Nimz, O.; Gessler, K.; Uson, I.; Saenger, W. *Carbohydr. Res.* **2001**, *336*, 141–153.

(4) Nimz, O.; Gessler, K.; Uson, I.; Laettig, S.; Welfle, H.; Sheldrick, G. M.; Saenger, W. *Carbohydr. Res.* **2003**, *338*, 977–986.

(5) Nimz, O.; Gessler, K.; Uson, I.; Sheldrick, G. M.; Saenger, W. *Carbohydr. Res.* **2004**, *339*, 1427–1437.

(6) Ivanov, P. M.; Jaime, C. *J. Phys. Chem. B* **2004**, *108*, 6261–6274.

(7) Schnupf, U.; Willett, J. L.; Momany, F. A. *Carbohydr. Res.* **2009**, *344*, 374–383.

(8) Schnupf, U.; Willett, J. L.; Momany, F. A. *J. Comput. Chem.* **2011**, *31*, 2087–2097.

(9) Momany, F. A.; Willett, J. L. *Carbohydr. Res.* **2000**, *326*, 210–226.

(10) Grimme, S. *J. Comput. Chem.* **2006**, *27*, 1787–1799.

(11) Cossi, M.; Barone, V.; Cammi, R.; Tomasi, J. *Chem. Phys. Lett.* **1996**, *255*, 327–335.

(12) Elstner, M.; Porezag, D.; Jungnickel, G.; Elsner, J.; Haugk, M.; Prauenheim, Th.; Suhai, S. *Phys Rev. B* **1998**, *58*, 7260–7268.
(13) Frisch, M. J.; Trucks, G. W.; Schlegel, H. B.; Scuseria, G. E.; Robb, M. A.; Cheeseman, J. R.; Montgomery, J. A., Jr.; Vreven, T.; Kudin, K. N.; Burant, J. C.; Millam, J. M.; Iyengar, S. S.; Tomasi, J.; Barone, V.; Mennucci, B.; Cossi, M.; Scalmani, G.; Rega, N.; Petersson, G. A.; Nakatsuji, H.; Hada, M.; Ehara, M.; Toyota, K.; Fukuda, R.; Hasegawa, J.; Ishida, M.; Nakajima, T.; Honda, Y.; Kitao, O.; Nakai, H.; Klene, M.; Li, X.; Knox, J. E.; Hratchian, H. P.; Cross, J. B.; Bakken, V.; Adamo, C.; Jaramillo, J.; Gomperts, R.; Stratmann, R. E.; Yazyev, O.; Austin, A. J.; Cammi, R.; Pomelli, C.; Ochterski, J. W.; Ayala, P. Y.; Morokuma, K.; Voth, G. A.; Salvador, P.; Dannenberg, J. J.; Zakrzewski, V. G.; Dapprich, S.; Daniels, A. D.; Strain, M. C.; Farkas, O.; Malick, D. K.; Rabuck, A. D.; Raghavachari, K.; Foresman, J. B.; Ortiz, J. V.; Cui, Q.; Baboul, A. G.; Clifford, S.; Cioslowski, J.; Stefanov, B. B.; Liu, G.; Liashenko, A.; Piskorz, P.; Komaromi, I.; Martin, R. L.; Fox, D. J.; Keith, T.; Al-Laham, M. A.; Peng, C. Y.; Nanayakkara, A.; Challacombe, M.; Gill, P. M. W.; Johnson, B.; Chen, W.; Wong, M. W.; Gonzalez, C.; Pople, J. A. *Gaussian 03*, revision A.1; Gaussian, Inc;: Pittsburgh, PA: 2004.
(14) *PQS Ab Initio Program Package*; Parallel Quantum Solutions: Fayetteville, AR, 2006.
(15) Cramer, D.; Pople, J. A. *J. Am. Chem. Soc.* **1975**, *97*, 1354–1358.
(16) Takahashi, Y.; Kumano, T.; Nishukawa, S. *Macromolecules* **2004**, *37*, 6827–6832.
(17) Sarko, A., Zugenmaier, P. In *Fiber Diffraction Methods*; French, A. D., Gardner, K. C. H., Eds.; ACS Symposium Series; American Chemical Society: Washington, DC, 1980; No. 141, pp 459−482.
(18) Rappenecker, G.; Zugenmaier, P. *Carbohydr. Res.* **1981**, *89*, 11–19.
(19) Murphy, V. G.; Zaslow, B.; French, A. D. *Biopolymers* **1975**, *14*, 1487–1501.
(20) Veregin, R. P.; Fyfe, C. A.; Marchessault, R. H. *Macromolecules* **1987**, *20*, 3007–3012.
(21) Gidley, M. J.; Bociek, S. M. *J. Am. Chem. Soc.* **1988**, *110*, 3820–3829.